

FLUKA: Performances and Applications in the Intermediate Energy Range

A. Fassò

CERN, 1211 Geneva 23, Switzerland

A. Ferrari, J. Ranft, P.R. Sala

INFN, Sezione di Milano, Via Celoria 16, 20133 Milano, Italy

Abstract

The FLUKA Monte Carlo code has been recently improved in the low and in the intermediate energy range. New physical models have been implemented concerning both hadronic and electromagnetic interactions, and neutron transport has been extended to thermal energies. The code has also been provided with powerful variance reduction options, which make it very suitable for deep penetration calculations. Thanks to all these new features FLUKA is now especially adapted to solve problems connected with accelerators of the new generation, not only in the shielding domain but also in that of particle physics, waste transmutation, radiotherapy, and synchrotron radiation.

1. Introduction

A new generation of intermediate energy proton and electron accelerators is under construction or planned in the near future. Shielding designers are confronted with a double challenge, due to *i)* the lack of reliable data in the energy range 20 MeV–1 GeV (source terms, attenuation lengths, angular and energy distributions of secondary particles) and *ii)* the difficulty of assessing correctly the large shield thicknesses required by the high beam intensity of most of the planned facilities. Compared with both the lower and higher energy range, where a considerable body of knowledge has been accumulated (see for instance [1, 2]) and sophisticated computing tools have existed and have been continuously updated since several decades [3, 4, 5], shielding of intermediate energy accelerators is still relying mostly on scattered empirical information (for a review see [6, 7, 8]). Many of the transport codes available are based on physical models which are more than 20 years old [9], and being strictly analog are not well suited for deep penetration calculations.

A good knowledge of radiation transport in the low and intermediate energy range is critical also for other activities which apparently have very little in common with the new medical and industrial accelerators. Radiation background in the large experiments which are currently planned to be installed at the future LHC proton-proton collider will be dominated by particle fluxes which can only be estimated by simulation of the whole hadronic cascade from several TeV down to thermal energies. Most of the particle production will take place at energies below 1 GeV. A similar situation arises in the assessment of the radiation dose affecting the crew of commercial airplanes or of space stations.

Detailed physical models in this energy range are also required when designing and operating experiments based on calorimetry. Missing p_t measurements and CP violation experiments are very sensitive to the response of calorimeters to relatively low energy hadrons. A detailed comprehension of calorimeter responses to subGeV hadrons will be a key issue for many of the future experiments.

Recently, new possibilities have emerged in this domain with the improvements of the code FLUKA in the range of energies below 1 GeV. For many years that program has been known as one of the main tools for designing shielding of proton accelerators in the multi-GeV energy range (its hadron event generator [10] has been adopted by the majority of the existing high-energy transport codes [11, 12, 13], including those used for particle physics simulations [14, 15]). In the last years, however, FLUKA has gone through an important process of transformation which has converted it from a specialized to a multi-purpose program, not restricted to a limited family of particles or to a particular energy domain.

In the course of this important development, no effort has been spared to keep the program structure as uniform and self-consistent as possible. The same attention has been devoted to each component of the hadronic and of the electromagnetic cascade, with the aim of obtaining a similar degree of accuracy for all of them. For this reason, FLUKA can be used just as well to solve problems where only a single component is present (pure hadron, neutron, muon or electromagnetic problems). It has also been tried to give a complete description of the mutual interaction between the different components, preserving the possible correlations. In this sense the new FLUKA is a really *complete* transport program. It doesn't neglect kaons, hyperons and antiparticles. It can generate and transport the photons due to π^0 decay and to nuclear de-excitation as well as neutrons and other hadrons produced by photons in nuclear reactions.

If in its original high energy field FLUKA has few competitors, this is not the case in the intermediate and in the low energy range, where several well established transport codes exist. However, FLUKA can compare favourably with most of them, thanks to some important assets. One of them is the adoption of modern physical models, especially in the description of nuclear interactions. Some of these models have even been updated and extended with original contributions. Other advantages are the special care devoted to low-energy electromagnetic effects and the accurate combined treatment of multiple scattering and magnetic fields near material boundaries, essential for a correct simulation of many synchrotron radiation problems.

The greatest importance has been attached to numerical accuracy: the whole code, including the random number generator, is in double precision and energy conservation is ensured within 10^{-10} . The program is also comparatively efficient, thanks to a careful choice of sampling algorithms (table lookup has been privileged). An ample supply of biasing options makes it possible to handle even problems of

very deep penetration in reasonable computing times, and several new strategies have been devised to boost geometry tracking performance, in particular when repetitive geometry structure are present.

Last but not least, FLUKA is still comparatively easy to use. This is not completely true if the user wishes to take a full advantage of all its most advanced features: but reasonable defaults allow most problems to be solved without having to write a single line of code. Input preparation may take a few hours or a few days depending on the complexity of the problem. However, a simple knowledge of programming may be useful to analyze some of the output.

The potential usefulness of FLUKA in the intermediate energy range is not confined to shielding. The background problems at high-energy colliders and the irradiation of airplane crews have already been mentioned, but recent applications have been successful also in fields as diverse as nuclear waste transmutation and accelerator-driven energy production, vacuum chamber engineering in intense synchrotron radiation environments, and design of underground physics experiments. The capabilities and the accuracy of the program recommend it also for radiotherapy planning (with any kind of radiation) and for dosimetry and detector studies.

2. Particles transported and interaction models

FLUKA can transport all neutral and charged hadrons which are stable under strong decay. In the energy range under consideration the only relevant particles for the hadronic sector are nucleons and pions.

2.1. Preequilibrium region: the PEANUT code

The intermediate energy event generator implemented in FLUKA87 [16] was based on the production and decay of one or more resonances to model the primary hadron-nucleon interactions, coupled to a parametrized nuclear cascade. Despite many improvements in the parametrizations, in the kinematics and in the treatment of nuclear effects, [5, 10, 17] it became increasingly inaccurate at energies lower than about 1 GeV. Therefore, in the last years it has been gradually substituted in FLUKA by the model called PEANUT (for PreEquilibrium Approach to NUclear Thermalization). Indeed, a correct treatment of the nuclear thermalization process including a preequilibrium stage is still missing in most Monte Carlo codes, except LAHET which includes a specialized algorithm [13], and GEANT, in which an older version of PEANUT [18] has been implemented. Presently, PEANUT handles interactions of nucleons, pions and γ rays with nuclei from about 1 GeV down to reaction threshold (or 20 MeV for neutrons). As concerns photonuclear reactions, details can be found in [19].

2.1.1 Description

The reaction mechanism is modelled in PEANUT by explicit intranuclear cascade (INC, first implemented as a Monte Carlo by Metropolis [20], see also Bertini [9]) smoothly joined to statistical (exciton) preequilibrium emission [21, 22]. The full INC treatment stops, and the statistical treatment starts, when all the secondary nucleons have energies smaller than 50 MeV (as calculated in the continuum). To ensure continuity, however, secondary nucleons with $10 < E < 50$ MeV are transported by the INC algorithm till they either escape or reinteract in the nucleus. In the latter case no explicit interaction is performed: only an average Pauli rejection factor [23] is applied and the exciton number is increased.

In both stages, INC and exciton, the nucleus is modelled as a sphere with density given by a symmetrized Woods-Saxon [24] shape with standard parameters. It is radially divided in 14 zones of constant density, and its boundary is set at the radius (R_{nuc}) where the density is one hundredth of the central one. Binding Energies (B.E.) are obtained from mass tables, depending on particle type and on the actual composite nucleus, which may differ from the initial one in the case of multiple particle emission. Relativistic kinematics is applied, with accurate conservation of energy and momentum, and with inclusion of the recoil energy and momentum of the residual nucleus.

The exciton formalism employed here follows that of M. Blann and coworkers [25, 26, 27, 28], called Geometry Dependent Hybrid Model (GDH). Indeed there are a few modifications, regarding mainly

inverse cross sections and exciton reinteraction rates. Inverse cross section were fitted to available experimental data. For the exciton reinteraction rate nucleon-nucleon cross section corrected [23] for Fermi motion and Pauli principle, have been used. Further corrections connected to nucleon correlations and to coherence considerations after scattering events have been introduced when computing the reinteraction rate, for consistency with what is done in the INC part (see the next paragraph). These corrections proved to be very useful and prevented the need for arbitrary reduction factors of the nucleon-nucleon cross sections, which were often required in similar models to match the experimental data.

A non-isotropic angular distribution has been implemented, following the fast particle approximation [29], as implemented by Akkermans *et al.* [30]. In this model the angular orientation of the nucleus at each step is defined by the direction of the fast particle, which changes gradually in a series of two-body collisions. The transition rate between different exciton states is supposed to be factorizable in an energy-dependent and an angle-dependent factor. The same factorization holds then for the resulting emission probability :

$$\frac{dP_{x,n,\theta}(\epsilon)d\epsilon}{d\Omega} = P_{x,n}(\epsilon)d\epsilon \cdot \sum_l a_l^m P_l(\cos(\theta)) \quad (1)$$

where $P_{x,n}(\epsilon)d\epsilon$ is the angle-integrated emission probability from an n-exciton state as given by GDH, the a_l^m are coefficients that depend on the number of steps m in the exciton chain, and θ in the original formulation is the polar angle with respect to the direction of the projectile. Since in PEANUT the exciton stage may be reached after one or more cascade steps, possibly with particle emission, care must be taken in defining the initial step number and the reference direction. The choice has been to define the reference axis as that of the residual momentum of the system at the step under consideration (it coincides with that of the projectile if no particles have been yet emitted). If this total momentum is comparable with the average Fermi momentum, the angular distribution is assumed to be isotropic. As for the step number m , it is taken equal to the number of holes below the Fermi level.

In the INC algorithm, both transport and interactions have been carefully modelled.

All particles are transported along paths which are subject to curvature in the Coulomb and nuclear potentials. In this way, refraction and reflection at the nuclear surface are taken into account, and the Coulomb effects are properly described. The potential used for nucleons has been found to have a strong influence on the results: a careful investigation of different options is still going on, and a definitive choice has not yet been made. Energy dependent as well as constant potentials with different depths and radial profiles can be managed by the model. At the moment, the standard one, used throughout this paper, is essentially the Fermi potential, *i.e.* a potential given by the Fermi gas relation between density and potential well:

$$E_F(r) = -(V(r) + B.E.) = \left(\frac{3\pi^2}{2}\right)^{\frac{2}{3}} \frac{\rho^{\frac{2}{3}}(r)}{2M} \quad (2)$$

It is clear from eq. 2 that $V(r)$ equals the binding energy at the nuclear outer radius. From here it is forced to go to zero in six additional radial intervals. For the Coulomb potential, eight zones have been added to calculate trajectories of outgoing particles up to the radius at which the potential is 1/10 of its value at the barrier, while Coulomb deflections of incoming particles are computed analytically solving the (relativistic) equation of motion up to the radius where the nuclear potential starts.

For pions, a nuclear potential has been calculated starting from the standard pion-nucleus optical potential [31]. In coordinate space, and in the frame in which the nucleus is at rest, this is written as (the upper and lower signs refer to π^+ and π^- , respectively, while π^0 's are not sensitive to N-Z asymmetry):

$$2\omega U_{opt}(\omega, r) = -\beta - \nabla \cdot \frac{\alpha}{1 + g\alpha} \nabla + \frac{\omega}{2M} \nabla^2 \alpha \quad (3)$$

$$\beta = 4\pi \left[\left(1 + \frac{\omega}{M}\right) \left(b_0(\omega) \mp b_1(\omega) \frac{N-Z}{A}\right) \rho(r) + \left(1 + \frac{\omega}{2M}\right) B_0(\omega) \rho^2(r) \right] \quad (4)$$

$$\alpha = 4\pi \left[\frac{1}{1 + \frac{\omega}{M}} \left(c_0(\omega) \mp c_1(\omega) \frac{N-Z}{A}\right) \rho(r) + \frac{1}{1 + \frac{\omega}{2M}} C_0(\omega) \rho^2(r) \right] \quad (5)$$

where ω is the first component of the pion 4-momentum, M is the nucleon mass, U_{opt} is the optical potential, $b_0, b_1, c_0, c_1, B_0, C_0$ are complex parameters, g is the Lorentz-Lorenz correction parameter [31]

(here and in the following the natural system of units , $\hbar c = 1$, is used). The functional form of this potential derives from that of the pion-nucleon scattering amplitude: b 's are related to s-wave pion-nucleon interaction, while c 's are related to p-wave interaction. The terms in ρ^2 account for two-nucleons mechanisms. This potential is non-local, thus a semiclassical approximation is in principle not possible. However, many localization procedures have been already devised for it [32, 33, 34]. As a result, we can re-write it:

$$2\omega U_{opt}(\omega, K) = -\beta - K^2 \frac{\alpha}{1 + g\alpha} + \frac{\omega}{2M} \nabla^2 \alpha \quad (6)$$

where K is the pion wave number inside the nucleus and the nuclear density that enters in α and β is the local one. In the literature, the Klein-Gordon equation for the pion in the nuclear optical potential is always written as:

$$[(\omega - V_c)^2 - 2\omega U_{opt}] - K^2] \Psi = m_\pi^2 \Psi \quad (7)$$

From eq. 7 applying energy conservation and calling k_0 the linear momentum of the pion outside the potential range, one obtains an equation for K^2 :

$$K^2 = k_0^2 + V_c^2 - 2\omega V_c - 2\omega U_{opt}(\omega, K) \quad (8)$$

substituting eq. 6

$$K^2 = \frac{k_0^2 + V_c^2 - 2\omega V_c + \beta - \frac{\omega}{2M} \nabla^2 \alpha}{1 - \bar{\alpha}} \quad (9)$$

$$\bar{\alpha} = \frac{\alpha}{1 + g\alpha} \quad (10)$$

The real part of K^2 gives then the real part of the potential from eq. 8. As pointed out by Johnson and Bethe [35], the denominator of eq. 9 approaches zero for normal nuclear densities. In ref. [35, 36] they suggested a correction which takes into account the effects of correlated scattering centers, and reduces the values of the potential as the density increases. This correction has been applied here to the p-wave part of the potential.

Moreover, eq. 7 is an approximation of the complete Klein Gordon equation, obtained dropping the terms of order U^2 . These terms are, however, negligible only at low pion energies, but not near resonance, where the potential itself can be comparable to the pion mass. Therefore we introduced in our transport equations a potential V_{opt} such as to satisfy

$$[(\omega - V_c - V_{opt})^2 - K^2] = m_\pi^2 \quad (11)$$

Comparing eq. 7 and eq. 11 one finds the relation between U_{opt} and V_{opt} :

$$V_{opt} = (\omega - V_c) - \sqrt{(\omega - V_c)^2 - 2\omega U_{opt}} \quad (12)$$

The values of the optical potential parameters at low energies (below 50 MeV) are known [31, 37] from pionic atoms and scattering data. At higher energies, however, only an extrapolation based on pion-nucleon phase shifts is available [37]. In this work, a fit of the values of ref. [37] has been used for the s-wave parameters, while for the dependence of the p-wave parameters on energy a resonant shape has been assumed, following the theoretical behaviour of the pion-nucleon scattering amplitude, which is dominated by the Δ resonance channel. Correction factors have been applied to account for the difference between the Δ width in nuclear matter and the free one due to Pauli principle, two body absorption and Fermi motion [33, 38, 39]. Care has been taken to obtain the standard values at low energies.

Path lengths and interaction mechanisms for all particles transported are chosen depending on particle-nucleon cross sections and local density. A rejection method is applied to take into account the dependence of the center of mass energy, and correspondingly of the cross section, on the actual momentum of the struck nucleon. The latter is, in turn, chosen according to a local Fermi distribution. Moreover, all secondary nucleons are required to satisfy the Pauli exclusion principle; if they don't, the interaction is rejected.

Mechanisms other than Pauli blocking which could be effective in increasing the particle mean free path in nuclear medium have been investigated and implemented. These mechanisms are important to prevent the well known problems [40] met by INC codes including refraction and reflection because of strong secondary absorption in the nucleus core. The following mechanisms are implemented into PEANUT:

- The formation zone [41] concept after pion or nucleon inelastic (pion production) interactions
- Nucleon antisymmetrization effects [42], which decrease the probability for secondary particles to reinteract on a nucleon of the same type very close to the production point
- Nucleon-nucleon hard-core correlations (see for example [43]) which also prevent secondary particles to collide again too close to the production point. Typical hard-core radii used in PEANUT are in the range 0.5-1 fm
- "Coherence" length after elastic or charge exchange hadron-nucleon scatterings. In analogy with the formation zone concept, such interactions cannot be localized better than the position uncertainty connected with the four-momentum transfer of the collision. Reinteractions occurring at distances shorter than the coherence length would undergo interference and cannot be treated anyway as independent interactions on other nucleons. Therefore in PEANUT particles are not allowed to reinteract within such a distance. It must be stressed that this mechanism is rather selective on the outgoing direction. Forward scattered particles are preferably emitted as well as backward scattered ones if the colliding particles are identical, pp or nn for example.

Nucleon-nucleon total cross sections, both elastic and inelastic, are taken from available experimental data. Elastic scattering is explicitly performed according to the experimental differential cross sections. Inelastic scattering (pion production) is handled by the HADRIN [44] model through the formation and decay of resonances.

Pion induced reactions are more complex, mainly because of the two-and three-body absorption processes. Above the pion production threshold, the inelastic interactions are, again, handled by HADRIN. Other pion-nucleon interactions proceed through the non-resonant channel and the p-wave channel with the formation of a Δ resonance. In nuclear matter, the Δ can either decay, resulting in elastic scattering or charge exchange, or interact with other nucleons, resulting in pion absorption. The width of the resonance is thus different from the free one. To account for this, the pion-nucleon total cross section used in PEANUT has been derived from the free one [45] in the following way: first, the resonant part has been extracted from the free cross section assuming for it a Breit-Wigner shape with an energy-dependent width as suggested by Ginocchio [46]

$$\sigma_r = \frac{8\pi}{p_{cm}^2} \frac{M_\Delta^2 \Gamma_F^2}{(s - M_\Delta^2)^2 + M_\Delta^2 \Gamma_F^2} \quad (13)$$

where p_{cm} is the pion momentum in the pion-nucleon center of mass system, s is the invariant mass squared, and $M_\Delta = 1.232$ GeV) Subtracting σ_r from the total experimental one, the non resonant scattering cross section σ_s is obtained. After that, a "new" resonant cross section σ_r^A is calculated adding to the free width Γ_F in eq. 13 the imaginary part of the (extra) width arising from nuclear medium effects. To this purpose the approach outlined in [38] has been adopted. The Δ effective width thus becomes:

$$\frac{1}{2}\Gamma_T = \frac{1}{2}\Gamma_F - Im\Sigma_\Delta \quad (14)$$

$\Sigma_\Delta = \Sigma_Q + \Sigma_2 + \Sigma_3$ as calculated by Oset et.al. [38]; Σ_Q , Σ_2 and Σ_3 are the partial widths for quasielastic scattering, two body and three body absorption (see ref. [38] for details). The partial resonant cross section for each channel is obtained from σ_r^A multiplying by the ratio $\frac{\Gamma_i}{\Gamma_T}$ ($\Gamma_i = \Gamma_F$ or $2\Sigma_2$ or $2\Sigma_3$). In addition, a two-body s-wave absorption cross section has been derived from the optical model [31] as

$$\sigma_s^A(\omega) = \frac{4\pi}{p} \left(1 + \frac{\omega}{2m}\right) ImB_0(\omega)\rho \quad (15)$$

The effective in-nucleus cross section has been thus recalculated as

$$\sigma_t^A = \sigma_r^A + \sigma_s + \sigma_s^A \quad (16)$$

Isospin relations have been extensively applied both to derive the pion-nucleon cross sections in any given charge configuration from the three experimentally known, and to weight the different interaction and decay channels of the Δ resonance [46, 47]. In s-wave absorption, the relative probability of absorption on a np pair or on a nn or pp pair, is assumed to be the same as in p-wave absorption. In the case of resonant reaction, the Δ is allowed to travel inside the nucleus according to its mean life $\tau_\Delta = \frac{\hbar}{\Gamma_\Delta}$ before decaying.

The angular and energy distribution of secondaries is essentially the experimental one for elastic and charge exchange scattering, while it is defined by phase-space considerations for two and three body absorption. It is planned to introduce for two body resonant absorption proper angular distributions based on experimental data on pion absorption on d and ^3He .

2.1.2 Benchmarks

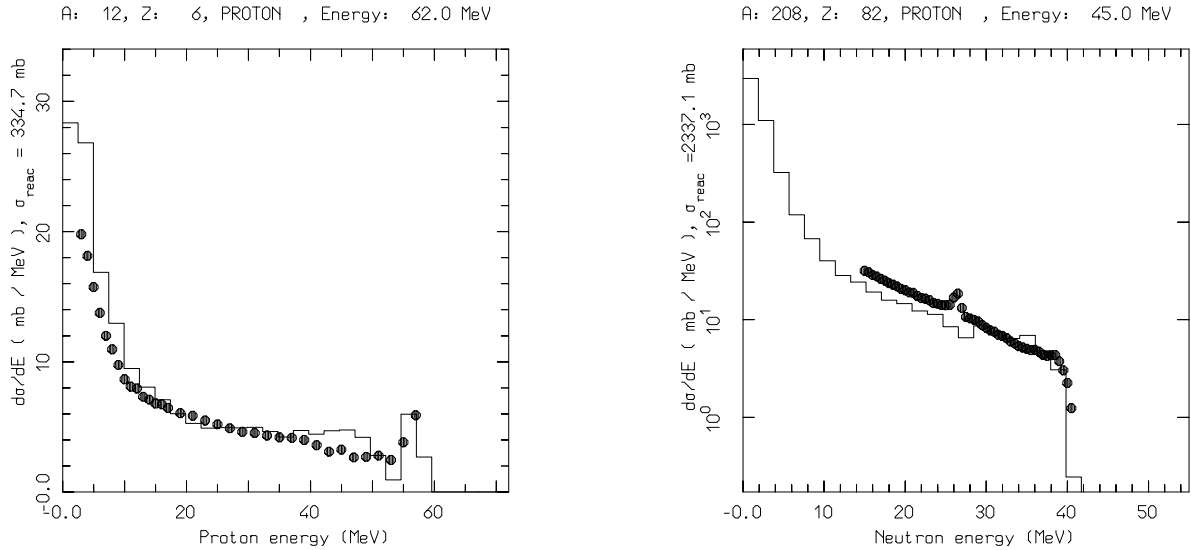


Figure 1: **Left** : proton spectrum following the reaction $^{12}\text{C}(p,px)$ at 62 MeV. **Right**: neutron spectrum following the reaction $^{208}\text{Pb}(p,nx)$ at 45 MeV. Experimental data (points) and simulation (histograms).

PEANUT has been extensively tested as a stand-alone code. Here we report some representative examples. In fig. 1 and fig. 2 examples of the capabilities of the model for low energy nucleon-induced reactions are shown. Experimental data are from ref. [48, 49]. The emitted particle spectrum is well reproduced, even in the “hard” part, which is often underestimated by exciton models. The angular distribution of emitted protons is also very satisfactorily reproduced. It must be pointed out that the inclusion of refraction and reflection effects as well as of the “coherence” length in the INC formulation gives a major improvement, especially in the backward region. Going to higher energies, figs. 3 and 4 show double differential distributions of neutrons emitted from thin targets bombarded with protons. Again, the agreement with experimental data (from refs. [50, 51, 52]) is good, both in the regions below and above the pion production threshold. Slight discrepancies in the backward spectrum, like the overestimation at 800 MeV, can be easily cured using energy dependent potentials for nucleons. However such potentials can give drawbacks at the lowest energies, mainly connected to the ambiguity

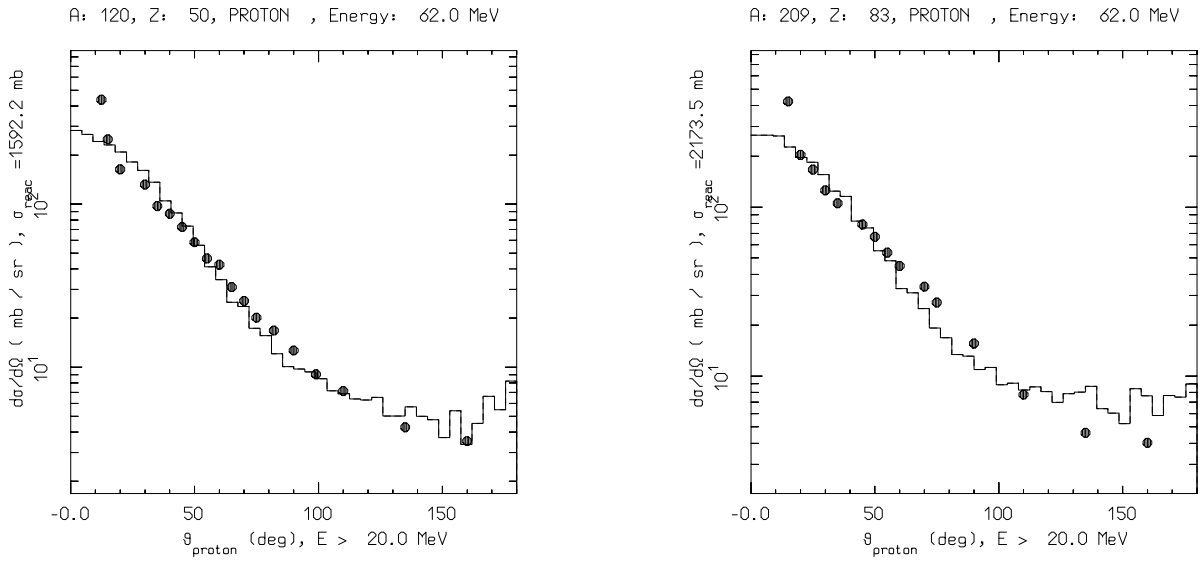


Figure 2: Angular distribution of protons following the reaction $^{120}\text{Sn}(p,px)$ (left) and $^{209}\text{Bi}(p,px)$ (right) at 62 MeV Experimental data (points) and simulation (histograms).

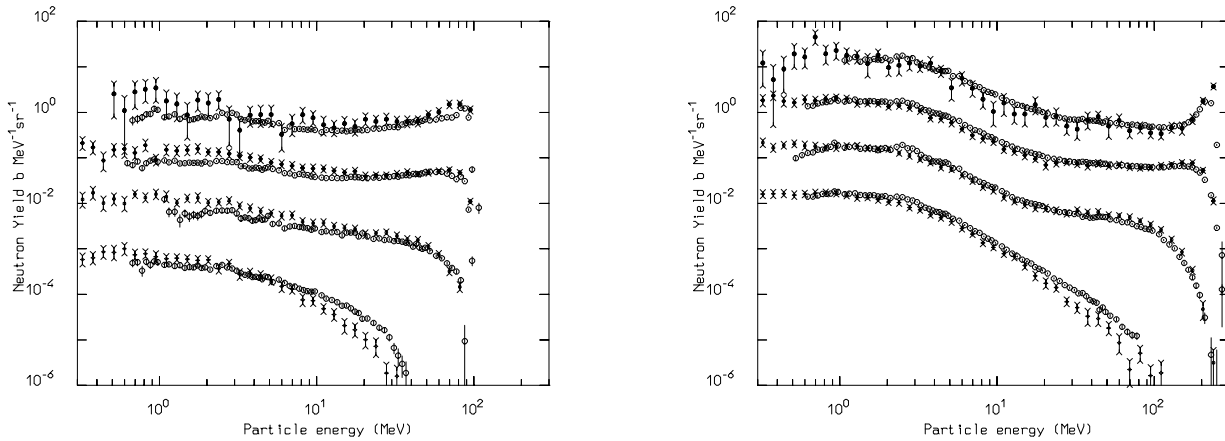


Figure 3: Neutron emission double differential cross sections for 113 MeV p on C (left) and 256 MeV p on Fe (right) at $7.5^\circ (\times 10^3)$, $30^\circ (\times 10^2)$, $60^\circ (\times 10)$ and 150° : experimental data (circles) and simulation (symbols with error bars) .

(in the INC part) in nucleon-nucleon collisions, where the center-of-mass energy is no longer the same before and after the collision. Work is in progress to identify possible solutions which could allow the use of such velocity dependent potentials.

Examples of the energy dependence of pion absorption cross section, of spectra of emitted nucleons, and of angular distributions of emitted pions after inelastic and charge exchange scattering are presented in figs. 5, 6 and 7. Model predictions are compared with data from [53, 54, 55, 56, 57, 58] and show agreement within the experimental uncertainties. The slight underestimation of forward emitted protons in fig 6 can be attributed to the lack of a realistic angular distribution in the two body absorption process.

While inelastic and charge exchange scatterings of positive pions are well reproduced for the full range of target masses, charge exchange of negative pions starts to deviate from experimental data for target masses above 100. The overestimation of π^- charge exchange cross sections on medium-heavy

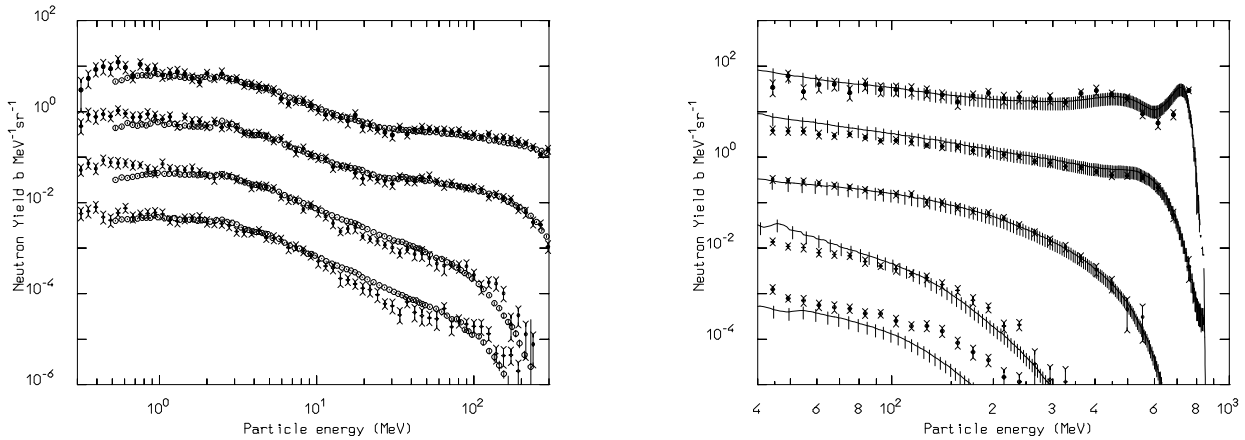


Figure 4: Neutron emission double differential cross sections for 597 MeV p on Al (left) and 800 MeV p on Pb (right) at $7.5^\circ (\times 10^4)$, only at 800 MeV, $30^\circ (\times 10^3)$, $60^\circ (\times 10^2)$, $120^\circ (\times 10)$ and 150° : experimental data (circles or dashed histogram) and simulation (symbols with error bars) .

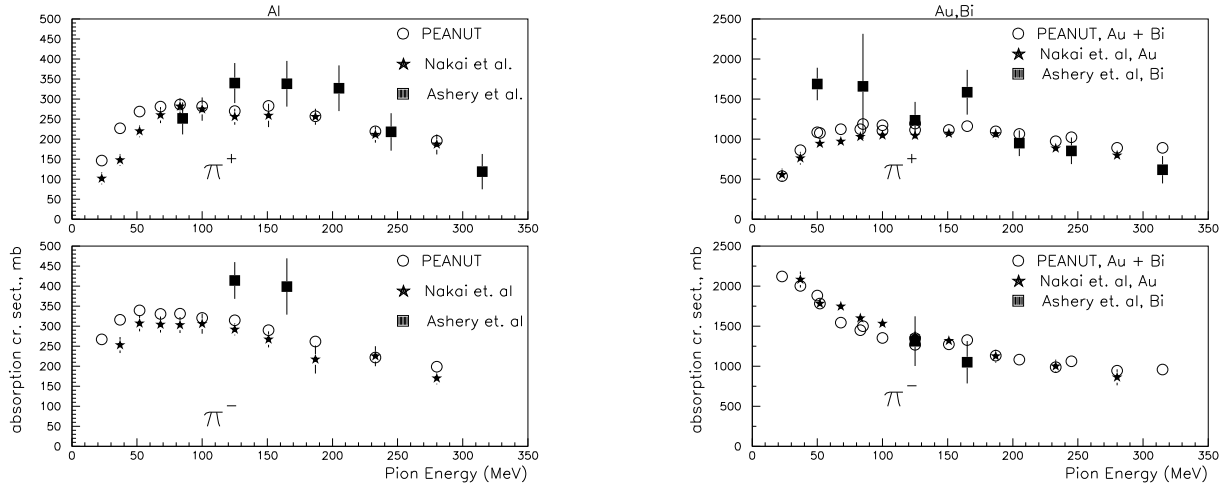


Figure 5: Pion absorption cross section on Aluminum (left) and Gold or Bismuth (right) as a function of energy

nuclei can be appreciated in fig. 8. A careful investigation of the available experimental data [54] shows a saturation of π^- charge exchange cross section for atomic numbers around 50 with possibly even a decrease for larger masses (see fig. 6 of ref. [54]). Such a behaviour, if confirmed, can hardly be obtained out of an INC model, and could point to more subtle interplays between quasi-elastic and absorption channels such as to inhibit selectively this specific reaction channel. This conclusion is also confirmed by the rather good agreement obtained for the angle integrated (no differential data have been found) negative pion inelastic cross section when compared with the values quoted in ref. [53]. At the lower edge of the mass range the absorption cross section predicted by the model seems to be somewhat low near resonance for very light elements such as Carbon, although the inelastic cross section appears to be correct (see fig. 9). Possibly an improvement could result from the introduction of a shell-model density distribution for light elements which is planned in the next months. However it must be pointed out that there exist discrepancies and inconsistencies among experimental data from different sources both for absorption and inelastic-charge exchange channels. Firm conclusions can be drawn only if further experimental data will become available. This is indeed a field where new measurements are welcome and required.

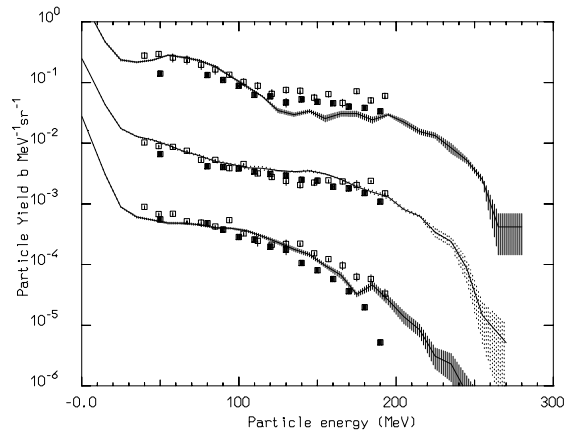


Figure 6: **Double differential spectra of protons emitted at 30° ($\times 10^2$), 60° ($\times 10$), 125° from a Nickel Target hit by 160 MeV π^+ . Points are experimental data, dashed histograms are calculations with errors**

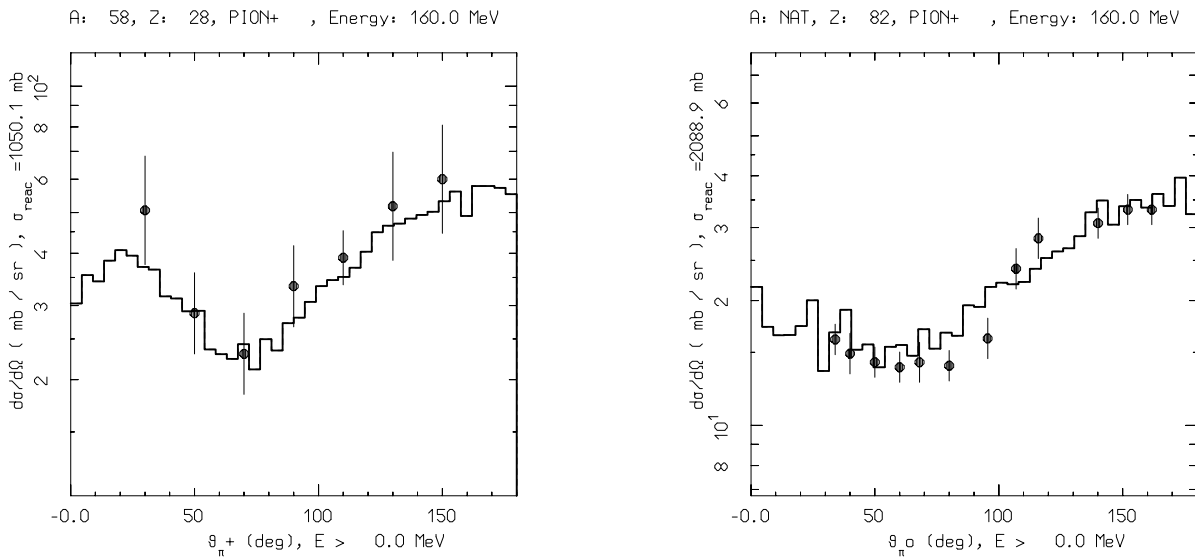


Figure 7: **Angular distribution of 160 MeV positive pions produced by inelastic scattering on Nickel (left) or charge exchange on Lead (right). Points are experimental data, histograms are PEANUT results**

2.2. Evaporation and fission

At the end of the exciton chain, the residual nucleus is a thermally equilibrated system with a certain amount of excitation energy, that can be spent in particle evaporation. The evaporative process is accomplished by a modified version of the EVAP-5 model from the HERMES code [12]. Modifications include different parametrizations of the level density now tabulated both with A and Z dependence and with the high temperature behaviour suggested by Ignatyuk [59], and the inclusion of relativistic kinematics.

The competition with fission has been recently included, following the fission algorithm of Atchison [60]

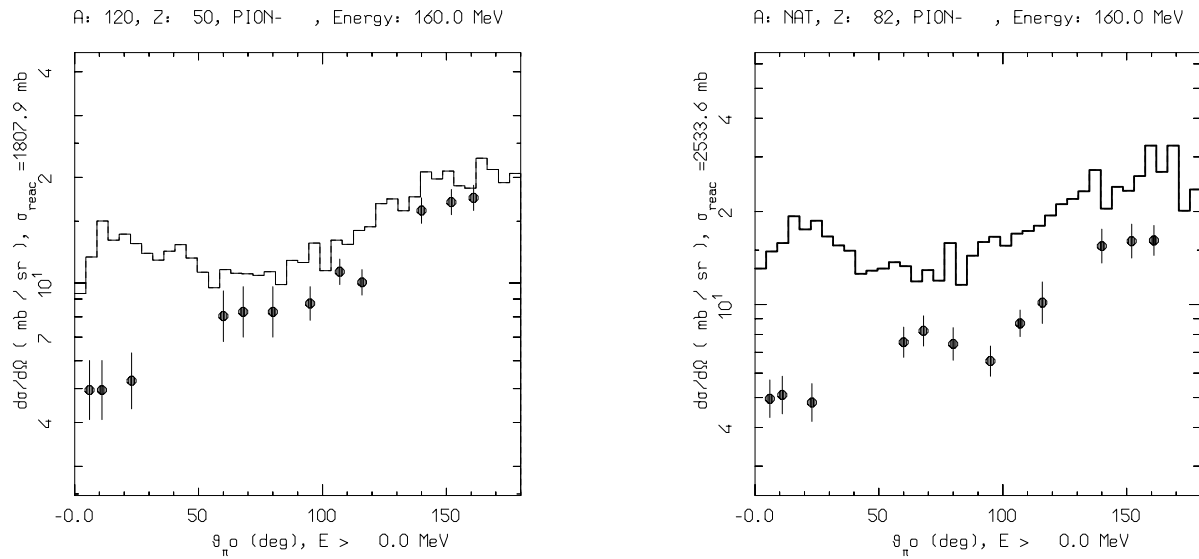


Figure 8: Angular distribution of pions produced by charge exchange of 160 MeV negative pions on Tin (left) and Lead (right). Points are experimental data, histogram are PEANUT results.

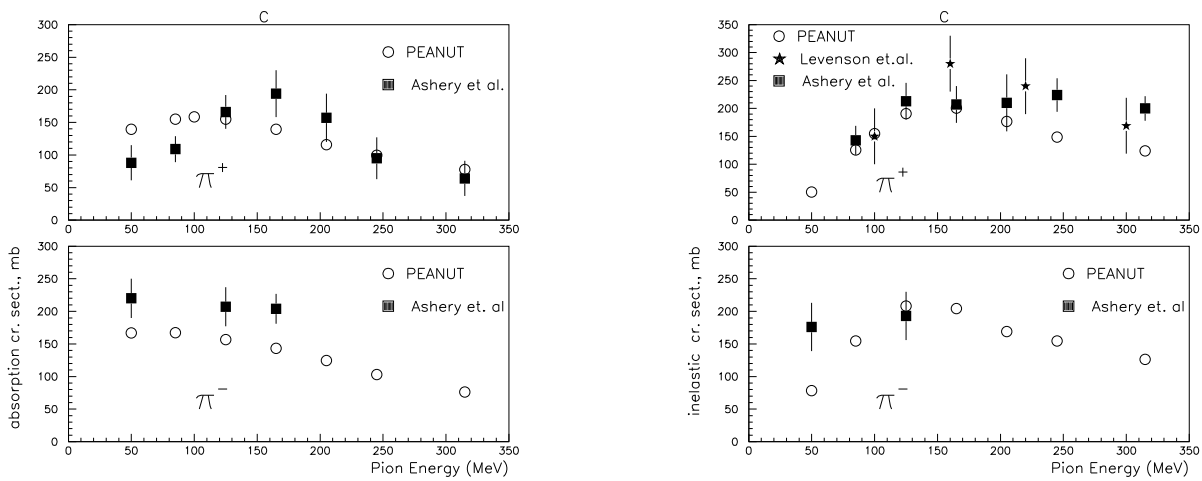


Figure 9: Absorption (left) and inelastic scattering (right) cross section for Carbon as a function of pion energy

as already implemented in LAHET.

A fragmentation model is still missing, therefore residual nuclei production is inaccurate very far from the target mass.

Finally, when the recoil excitation energy is lower than any particle emission threshold, a statistical gamma ray emission is simulated until the nucleus is left in its ground state.

2.3. Low-energy neutrons

A complete treatment of neutron propagation and slowing-down to thermal energies has replaced the 50 MeV energy cutoff of the previous FLUKA version. The multigroup approach is similar to that of

the MORSE code [61]. Calculations can proceed both in analog or biased fashion, depending on the user choice. Photons are generated according to the appropriate cross sections, but their transport is performed through the electromagnetic transport module of FLUKA (EMF). The energy deposition is usually computed using kerma factors but in the case of hydrogen the recoiling protons are explicitly generated and transported.

2.4. Electrons and photons

The part of FLUKA which has been most drastically modified in the last years is probably the transport

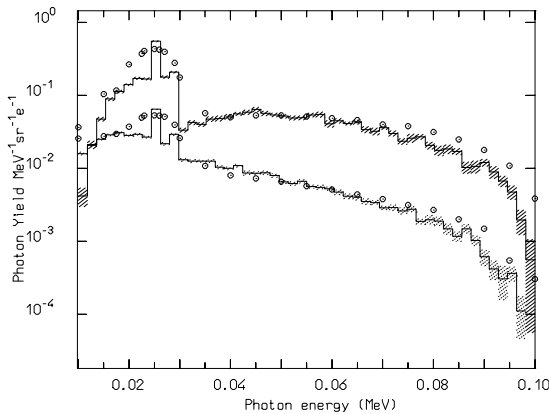


Figure 10: **Spectra of bremsstrahlung photons emitted at 70° ($\times 10$) and 110° from a thick Tin target hit by 100 keV electrons. Points: exp.data, dashed histogram: FLUKA**

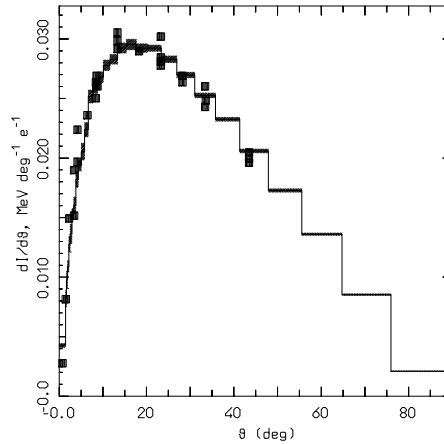


Figure 11: **Angular distribution of bremsstrahlung intensity from a thick Tantalum target hit by 10 MeV electrons. Points: exp.data, dashed histogram: FLUKA**

of electrons and photons. The old link with EGS4 has been completely replaced with a new code module with extended performance. As a result of the improvements, which have concerned most of the physical models used [62] and the whole charged particle tracking algorithm [63], FLUKA has become probably the only code which can simulate accurately cosmic ray showers up to energies of 1000 TeV [64] as well as energy deposition in thin layers and backscattering of electrons of few keV.

In FLUKA, photoelectric interactions are sampled separately for each component element and for each edge higher than 1 keV. Fluorescence and Auger electron emission are simulated for all K and most L lines, including the angular distribution of fluorescent photons (fully relativistic theory of Von Sauter).

Another very important process at intermediate energies is bremsstrahlung. Very accurate electron-nucleus and electron-electron bremsstrahlung cross sections, differential in photon energy and angle, have been published in recent years by Seltzer and Berger [65] for all elements up to 10 GeV, and have been introduced in their ETRAN code. In FLUKA the full set of Seltzer and Berger cross sections has been tabulated in extended form. The energy mesh has been concentrated, especially near the photon spectrum tip, and the maximum energy has been extended to higher energies. Positron bremsstrahlung is treated separately, using below 50 MeV the scaling function for the radiation integral given by Kim *et al.* [66] and differential cross sections obtained by fitting proper analytical formulae to numerical results of Feng *et al.* [67]. The photon angular distribution is obtained sampling the emission angle from the double differential formula reported by Koch and Motz [68], fully correlated with the photon energy sampled from the Seltzer-Berger distributions. Comparisons with experimental data (from refs. [69, 70]) are very satisfactory, as shown in figs. 10 and 11. A first application of this algorithm in a true accelerator environment has been recently made, showing very good agreement with data [71].

In pair production, angular and energy distributions are described in full detail, avoiding previous

approximations.

Compton scattering has also been re-written, taking into account the effect of electron binding .

3. PHYSICAL DATA AND LIBRARIES

A deliberate choice was made at an early stage to give preference to table look-up over analytical parametrizations or rejection sampling. The burden of large file management is more than compensated by the better accuracy and increased efficiency. Cumulative tabulations optimized for fast sampling are initialized at run-time for the materials of the problem on hand, and are obtained mainly from complete binary data libraries stored in external files. Only for a few basic quantities (cross sections, stopping powers) the tabulations are prepared from analytical fits to experimental data.

3.1. Neutron cross sections

The largest data file is a P5 multigroup neutron cross section library prepared with the help of an ENEA specialized laboratory [72]. Several versions are available. The simplest one has 37 neutron groups and 22 gamma groups (used only for gamma generation and not for transport), and is used mainly for routine shielding work. It contains about 75 different elements and single nuclides at different temperatures, selected among those which are most commonly needed for work on shielding, dosimetry and high-energy physics. The majority of the cross sections are derived from JEF-1, JEF-2.2 and ENDF/B-VI [73] evaluated files and include kerma factors (for energy deposition calculations) and partial cross sections. The latter are not used directly by FLUKA, but can be folded over calculated spectra to get reaction rates and induced activities. The same materials are also available in a file with a 72 neutron group structure. Only one thermal group is present in both libraries.

A completely new library is in preparation, based on the VITAMIN-J structure plus 20 thermal groups processed at different temperatures and different self-shielding factors in MATXS format. It is planned to use such a library to collapse smaller libraries for dedicated purposes.

3.2. Other libraries

Other physical data stored in external files include up-to-date values of nuclear masses and abundances, hadron cross sections, the extended Seltzer-Berger bremsstrahlung data and fluorescence information (K and L lines).

4. BIASING

Most high-energy transport codes are analog, *i.e.* designed to predict not only the average values of the physical quantities of interest, but also their variance and other moments of higher order. To this effect, all stochastic events are sampled according to their natural frequency of occurrence, resulting in a full *simulation* of the physical processes where correlations and random fluctuations are faithfully reproduced.

For many purposes however, and in particular in shielding design, the analog approach is inefficient because only macroscopic average quantities are important, which often result from the contribution of some statistically rare events. Therefore, specialized programs exist, like CASIM [74] and MARS [75], which make a systematic use of variance reduction techniques. Unlike low-energy Monte Carlo codes [61, 3], where transport biasing is under control of the user, the very structure of CASIM and MARS has been designed to take advantage of weighted sampling.

Still another line has been chosen in FLUKA. The user has the choice to use the code in a fully analog mode, or to apply a number of variance reduction techniques. The degree of biasing can be tuned as desired, on a region-by-region basis and in most cases also by particle. Under this aspect FLUKA is more similar to programs used for low-energy neutron and gamma shielding, and although very powerful for skilled shield designers, not all biasing options are entirely safe in the hands of an inexperienced user. This doesn't imply that FLUKA is only for experts: any beginner can safely run it in a pure analog mode and cautiously start exploring its deep-penetration possibilities.

4.1. *Surface splitting and Russian Roulette*

The simplest biasing option is the well-known splitting/Russian Roulette technique based on the concept of region "importance". The user assigns a numerical value to each geometry region (possibly modified depending on the type of particle). The number of particles of the selected type crossing a given boundary is reduced or increased on average by a factor equal to the ratio of the importances on either side of the boundary. What is relevant is the relative importance of different regions, not their absolute values. In simple deep-penetration problems, where only one main attenuation path is present, surface splitting is easy to use and very effective. In another paper presented at this Workshop, it is shown how good statistics can easily be attained with dose attenuation factors of the order of 10^{-6} .

4.2. *Weight window*

All biasing techniques (some more than others) introduce fluctuations of the particle statistical weight. A so-called "weight window" can be applied to damp such fluctuations within pre-defined limits. It is also based on Russian Roulette and splitting, but its application is not linked with geometrical boundaries and refers to the absolute value of the particle weight rather than to relative region importances. On the other hand, it can be used alone or in combination with surface splitting to control the size of particle population in different regions of space. Although less straightforward to apply than surface splitting, it can be finely tuned by region, particle and energy and increases the effectiveness of all other biasing techniques.

4.3. *Leading particle biasing*

Leading particle biasing is available only for electrons, positrons and photons, and is generally used to avoid the geometrical increase with energy of the number of particles in an electromagnetic shower. It is characteristic of all electromagnetic interactions that two particles are present in the final state: when this option is selected, only one of them (preferentially the most energetic one) is randomly retained and its weight is adjusted accordingly. Derived from the EGS4 [4] implementation, it has been modified to account for the indirectly enhanced penetration potential of positrons due to the emission of annihilation photons.

This kind of biasing is aimed at reducing the mean computing time per history rather than the variance of the scored quantities (computer cost is defined as the product of variance times the computing time per primary particle). It is mainly used to estimate shower punchthrough (but comparable and even better efficiency can be obtained with importance splitting), or to reduce the time spent in simulating secondary electromagnetic showers produced by π^0 in hadronic cascades. In the latter case, its interest is mainly at very high energies rather than at those which are of our concern here. When applied in energy deposition calculations, the use of weight windows is mandatory in order to avoid large local dose fluctuations.

4.4. *Biased downscattering*

The group-to-group transfer probabilities used in the transport of low-energy neutrons (the so called downscattering matrix) can be biased in order to artificially accelerate or slow down the moderation process. This option is difficult to use because it requires from the user a visualization of the particle path in phase space and of its projection on the energy axis, which can only be attained with a long experience. However, for a certain class of problems where moderation plays an important role, it can save considerable computer time. It should only be used with much care.

4.5. *Non-analog absorption*

This option too concerns the transport of low-energy neutrons. It is also called survival biasing. It is implemented in most low-energy neutron transport codes, where however the only choice left to the user is between analog absorption with the actual physical probability and systematic survival with a reduced weight. In FLUKA, as a third choice, the user is allowed to force the neutron absorption probability to assume an arbitrary value, pre-assigned on a region-by-region basis and for a selected number of energy groups. A small survival probability is often assigned to thermal neutrons in order to limit the number of scatterings in non-absorbing media; this option is also useful when dealing with materials with unusual scattering properties, such as iron. Use of a survival probability larger than the physical one is likely to introduce important weight fluctuations among different individual neutrons depending on the number of collisions undergone. To limit the size of such fluctuations, which could slow down statistical convergence, a weight window should be applied.

4.6. *Biased decay and interaction length*

The hadron mean free path for inelastic interaction can be artificially decreased in a given material (or in all materials) by a pre-defined particle dependent factor. This possibility is useful for instance to increase the probability of beam interaction in a very thin target or in a material of very low density. In a similar way, the mean life or the average decay length of unstable particles can be shortened, and it is also possible to increase the generation rate of decay products without actually stopping the parent particles (for example to enhance muon production statistics).

5. **GEOMETRY AND TRANSPORT**

The original Combinatorial Geometry (CG) by MAGI [76] has been modified in several ways. CG had originally been designed for neutral particles, but charged particles have required a more accurate treatment near boundaries, especially when magnetic fields are present.

New geometrical bodies have been added, making input preparation and debugging much easier and also saving much of the computer time spent in tracking.

The minimum distance to boundary has been implemented for most bodies, allowing the use of larger steps. More generally, the whole tracking strategy has been changed, achieving a considerable gain in speed.

Recent improvements include a simple debugging device which can be activated on request in order to check for non-assigned or for doubly-assigned parts of space, and the possibility to describe lattices or other repetitive structures that can be obtained by symmetry operations.

6. **CONCLUSIONS**

The new physical models recently implemented in FLUKA make it a good candidate for a variety of applications, well beyond its traditional domain. Successful experience has already been obtained with problems of bremsstrahlung and of synchrotron radiation related to several "factories" planned or under construction. Some attempts at using FLUKA for waste transmutation studies are underway and look rather promising, but probably some additional improvements in the physics of the nucleus will be necessary before the code can be considered fully reliable in this domain. Shielding of intermediate energy proton accelerators seems to be one of the most straightforward applications, as shown in another paper presented at this Workshop; but the capability of handling photonuclear reactions, very recently introduced, opens an even more interesting opportunity concerning shielding of electron accelerators.

The list could be further extended to calorimetry, accelerator-driven energy production (a study is going on at CERN), dosimetry (calculations of fluence to dose conversion factors), background studies for underground experiments, and, very likely in a near future, medical applications. Concerning the problem of air crews, FLUKA is currently being used to investigate a reference radiation field used for assessment of dosimetry techniques to be applied in this kind of studies. The list is not exhaustive, and more suggestions are expected soon; but a special mention must be made about the background and

radiation damage calculations for collider experiments, which have triggered most of the improvements described in this paper.

7. Acknowledgments

The authors are greatly indebted to P. A. Aarnio, G. R. Stevenson, H.-J. Moehring and J. M. Zazula who contributed a lot to the development of previous FLUKA versions. Many experimental data has been kindly made available to us by W. Scobel and R. E. Prael, who provided also the high energy fission model. The many useful discussions with G. Battistoni, who constantly stimulated FLUKA developments are also acknowledged. The essential contribution of G. C. Panini, who prepared the cross section data library is heartily thanked.

REFERENCES

1. A.B. Chilton, J.K. Shultis, R.E. Faw, "Principles of Radiation Shielding", Prentice-Hall, Englewood Cliffs 1984.
2. A. Fassò, K. Goebel, M. Höfert, J. Ranft, G.R. Stevenson, "Shielding Against High Energy Radiation" (ed. H. Schopper), *Landolt-Börnstein numerical data and functional relationships in science and technology*, **Vol. 11**, Springer Berlin 1990.
3. J.F. Briesmeister, editor "MCNP - A general Monte Carlo code for neutron and photon transport", Los Alamos report **LA-7396-M Rev.2** (1986)
4. W.R. Nelson, H. Hirayama and D.W.O. Rogers, "The EGS4 code system" Stanford Linear Accelerator Center report **SLAC-265** (1985).
5. A. Fassò, A. Ferrari, J. Ranft, P.R. Sala, G.R. Stevenson and J.M. Zazula, "FLUKA 92", *Proc. of the Workshop on Simulating Accelerator Radiation Environment*, Santa Fe, January 11-15, 1993 (in press).
6. R.H. Thomas and G.R. Stevenson, "Radiological safety aspects of the operation of proton accelerators", *IAEA Technical Report Series No. 283*, Vienna 1988.
7. W.P. Swanson, "Radiological safety aspects of the operation of electron linear accelerators", *IAEA Technical Report Series No. 188*, Vienna 1979.
8. "Neutron contamination from medical electron accelerators", *NCRP Report No. 79* (1984).
9. H.W. Bertini and M.P. Guthrie, "Results from medium-energy intranuclear-cascade calculation", *Nucl. Phys.* **A169**, 670 (1971).
10. A. Fassò, A. Ferrari, J. Ranft, P.R. Sala, G.R. Stevenson and J.M. Zazula, "FLUKA: hadronic benchmarks and applications", *Proc. of the MC93 Int. Conf. on Monte Carlo Simulation in High-Energy and Nuclear Physics*, Feb. 22-26, 1993. Ed. P. Dragovitsch, S.L. Linn, M. Burbank, World Scientific, Singapore, 1994 (p. 88).
11. R.G. Alsmiller, Jr., F.S. Alsmiller and O.W. Hermann, "The high-energy transport code HETC88 and comparisons with experimental data", *Nucl. Instr. Meth.* **A295**, 337 (1990).
12. P. Cloth *et al.*, "HERMES, a Monte Carlo program system for beam-materials interaction studies", *Jülich report KFA/Jül-2203* (1988).
13. R.E. Prael and H. Lichtenstein, "User guide to LCS: the LAHET code system", *Los Alamos report LA-UR-89-3014* (1989).
14. T.A. Gabriel, J.E. Brau and B.L. Bishop, "The physics of compensating calorimetry and the new CALOR89 code system", *Oak Ridge report ORNL/TM-11060* (1989).
15. R. Brun *et al.*, Report CERN DD/EE/84-1 (1987)
16. K. Hänssgen, H.J. Möhring and J. Ranft, *Nucl. Sci. Eng.* **88** (1984) 552.
17. A. Ferrari, P.R. Sala, A. Fassò and G.R. Stevenson, in *Proc. II int. Conference on Calorimetry in High Energy Physics*, ed. A. Ereditato, (World Scientific, 1992).

18. A. Ferrari and P.R. Sala, "A new model for hadronic interactions at intermediate energies for the FLUKA code", *Proc. of the MC93 Int. Conf. on Monte Carlo Simulation in High-Energy and Nuclear Physics*, Tallahassee, February 22-26, 1993. Ed. P. Dragovitsch, S.L. Linn, M. Burbank, World Scientific, Singapore, 1994 (p. 277).
19. A. Fassò *et al.*, *Proceedings of the Eighth Int. Conf on Radiation Shielding*, Arlington, Texas, April 24-28 1994.
20. N. Metropolis *et al.*, *Phys. Rev.* **110** (1958) 185.
21. J. J. Griffin, *Phys. Rev. Lett.* **17** (1966) 438.
22. E. Gadioli and P. E. Hodgson, *Pre-equilibrium Nuclear Reactions* Clarendon Press, Oxford (1992).
23. K. Kikuchi and M. Kawai, *Nuclear Matter and Nuclear Interactions* North-Holland, Amsterdam (1968).
24. M. E. Grypeos, G. A. Ialazisis, S. E. Massen and C. P. Panos *J. Phys* **G 17** (1991) 1093.
25. M. Blann, *Phys. Rev. Lett.* **27** (1971) 337.
26. M. Blann, *Phys. Rev. Lett.* **28** (1972) 757.
27. M. Blann and H.K. Vonach, *Phys. Rev.* **C28** (1983) 1475.
28. M. Blann, *Phys. Rev.* **C28** (1983) 1648.
29. G. Mantzouranis, D. Agassi, and H.A. Weidenmüller, *Phys. Lett.* **57B** (1975) 220.
30. J.M. Akkermans, H. Gruppelaar and G. Reffo, *Phys. Rev.* **C22** (1980) 73.
31. T. Ericson and W. Weise *Pions and Nuclei* (Clarendon Press, Oxford, 1988).
32. M. Krell and T.E.O. Ericson *Nucl. Phys.* **B11** (1969) 521.
33. J.N. Ginocchio and M.B. Johnson, *Phys. Rev.* **C21** (1980) 1056.
34. I.A. Lantsev and A.V. Pavlov *Sov. J. Nucl. Phys.* **54** (1991) 254.
35. M.B. Johnson and H.A. Bethe, *Nucl. Phys.* **A305** (1978) 418.
36. M.B. Johnson and B.D. Keister *Nucl. Phys.* **A305** (1978) 461.
37. K. Stricker, H. McManus, and J.A. Carr *Phys. Rev.* **C19** (1979) 929.
38. E. Oset and L.L. Salcedo, *Nucl. Phys.* **A468** (1987) 631.
39. L.L. Salcedo *et al.*, *Nucl. Phys.* **A484** (1988) 557.
40. K. Chen *et al.*, *Phys. Rev.* **166, 4** (1968) 949.
41. L. Stodolski, *Proc. Vth Int. Colloquium on Multiparticle Reactions*, Oxford (1975), 577.
42. A. Bohr, B.R. Mottelson, *Nuclear Structure Vol. 1*, W.A. Benjamin, Inc. (1969).
43. K. Chen *et al.*, *Phys. Rev.* **C4, 6** (1971) 2234.
44. K. Hänssgen and J. Ranft, *Nucl. Sci. Eng.* **88** (1984), 537.
45. Phase shift solutions KH78, KH80, in *Landolt-Börnstein, new series, Vol. 9, part II*, 1983.
46. J.N. Ginocchio, *Phys. Rev.* **C17** (1978) 195.
47. M.J. Vicente Vacas and E. Oset, *Nucl. Phys.* **A568** (1994), 855.
48. F.E. Bertrand, R.W. Peelle *Phys. Rev.* **C8** (1973), 1045.
49. A. Galonsky *et al.*, *Phys. Rev.* **C14** (1976), 748.
50. M.M. Meier, D.A. Clark, C.A. Goulding, J.B. McClelland, G.L. Morgan and C.E. Moss, *Nucl. Sci. and Eng.* **102** (1989), 310.
51. M.M. Meier, W.B. Amian, C.A. Goulding, G.L. Morgan and C.E. Moss, *Nucl. Sci. and Eng.* **110** (1992), 289.
52. S. Stamer *et al.*, G.L. Morgan and C.E. Moss, *Phys. Rev.* **C47, 3** (1993), 1647.
53. D. Ashery *et al.*, *Phys. Rev.* **C23** (1981), 2173.
54. D. Ashery *et al.*, *Phys. Rev.* **C30** (1984), 946.
55. K. Nakai *et al.* *Phys. Rev. Lett.* **44** (1979), 1446

56. S.M. Levenson *et al.*, *Phys. Rev.* **C28** (1983), 326.
57. W.J. Burger *et al.*, *Phys. Rev.* **C41** (1990) 2215.
58. R.D. McKeown *et al.*, *Phys. Rev.* **C24** (1981) 211.
59. A.V. Ignatyuk, G.N. Smirenkin and A.S. Tishin, *Sov. J. Nucl. Phys.* **21** (1975), 255.
60. F. Atchison, *Meeting on Targets for neutron beam spallation sources*, ed. G. Bauer, KFA Jülich Germany, **Jül-conf-34** 1980.
61. M.B. Emmett, *Report ORNL-4972* (1975).
62. P. A. Aarnio, A. Fassò, A. Ferrari, H.-J. Mörhing, J. Ranft, P.R. Sala, G.R. Stevenson and J.M. Zazula, *Proc. of the MC93 Int. Conf. on Monte Carlo Simulation in High-Energy and Nuclear Physics*, Feb. 22-26, 1993. Ed. P. Dragovitsch, S.L. Linn, M. Burbank, World Scientific, Singapore, 1994 (p. 100).
63. A. Ferrari, P.R. Sala, G. Guaraldi and F. Padoani, *Nucl. Instr. Meth.* **B71** (1992) 412.
64. V. Patera *et al.* *Simulation of the e. m. component of extensive air showers*, **LNF 94/015** (1994), submitted to *Nucl. Instr. Meth.*
65. S.M. Seltzer and M.J. Berger, *At. Data. Nucl. Data Tab.* **35** (1986) 345.
66. L. Kim *et al.*, *Phys. Rev.* **A33** (1986) 3002.
67. I.J. Feng, R.H. Pratt and H.K. Tseng, *Phys. Rev.* **A24** (1981) 1358.
68. H.W. Koch and J.W. Motz, *Rev. Mod. Phys.*, **314** (1959) 920.
69. M.J. Berger and S.M. Seltzer *Phys. Rev* **C2** (1970) 621.
70. R. Placious, *J. Appl. Phys.* **38** (1967) 2030.
71. A. Esposito, A. Ferrari, L. Liberatori and M. Pelliccioni, *Gas Bremsstrahlung: a Comparison of Measurements and Simulations*, submitted to *Nucl. Instr. Meth.*
72. E. Cuccoli *et al.*, *A group library from JEF 1.1 for flux calculations in the LHC machine detectors*, **JEF-DOC-340** (1991).
73. H.D. Lemmel, *Int. Atomic En. Agency Report* **IAEA-NDS-100** (1990).
74. A. Van Ginneken, *Fermilab report* **FN-272** (1975).
75. N.V. Mokhov, *Fermilab report* **FN-509** (1989).
76. W. Guber *et al.*, *Report* **MAGI-6701** (1967).